ISSN 2616-5880 Vol. 5, Issue 2: 29-36, DOI: 10.25236/AJMC.2024.050206

Theoretical study of Cu–Pd core–shell nanoparticles: structure, stability and electronic

Xueyan Hu, Yangyang Zhang[a,*], Xiaolei Zhao[b,*], Yulong Zhang

College of Chemistry and Chemical Engineering, Henan Polytechnic University, Jiaozuo, Henan, China
[a]yyzhang1991@126.com, [b]zhaoxiaolei@hpu.edu.cn
[*]Corresponding author

Abstract: *The bimetallic core–shell nanoparticles (CSNPs) exhibit superior stability, selectivity, and catalytic activity as well as display new functions owing to a lattice strain induced by the unique core-shell structures and synergistic effects of different metal components. These properties of bimetallic CSNPs can be tuned and expanded by varying the composition and atomic arrangement as well as their sizes, morphology, thickness, and sequence of both core and shell. In this study, the geometrical structure, thermodynamic stability, and electronic properties of 13- and 55-atom Cu, Pd nanoparticles (NPs), and Cu–Pd CSNPs were systematically investigated using density functional theory calculations. The results showed that Pd atoms prefer to segregate to the surface shell, while Cu atoms were inclined to aggregate in the core region for bimetallic Cu–Pd CSNPs; therefore, Cu@Pd CSNPs with a Pd surface-shell were thermodynamically more favourable than both the monometallic Cu/Pd NPs and the Pd@Cu CSNPs with a Cu surface-shell. The charge transfer increased from the Cu-core to the Pd-shell for the Cu@Pd CSNPs, while it decreased from the Pd-core to the Cu-shell for the Pd@Cu CSNPs. Opposite charge transfer in these CSNPs led to the Pd surface-shell that displays a negative charge, while the Cu surface-shell exhibits a positive charge.*

Keywords: *CSNPs, density functional theory, thermodynamic stability, electronic*

1. Introduction

The exploration of multifunctional bimetallic core-shell nanoparticles (CSNPs) has emerged as a pivotal research domain, driven by their fascinating physicochemical attributes and wide-ranging applications across catalysis, electrocatalysis, electronics, medical biotechnology, and beyond[1–3]. These bimetallic CSNPs offer enhanced stability, selectivity, and catalytic prowess, owing to lattice strain induced by their unique core-shell architectures and the synergistic interplay of diverse metal constituents. Notably, the properties of these CSNPs can be finely tailored and expanded by manipulating composition, atomic arrangement, as well as size, morphology, thickness, and sequence of both core and shell components[4–6]. Consequently, delving into the structural intricacies, stability, surface composition, electronic and magnetic characteristics, and catalytic behavior of CSNPs is pivotal for advancing the frontiers of heterogeneous catalysis and materials chemistry.

Cu-Pd core-shell nanoparticles (CSNPs) are a type of nanostructured material composed of a copper (Cu) core covered with a thin shell of palladium (Pd)[7]. The incorporation of Cu and Pd into these nanoparticles offers a synergistic effect, combining the electrical conductivity of Cu with the catalytic activity of Pd[8]. This combination not only enhances the reactivity of the nanoparticles but also broadens their potential applications in various fields.

Cu-Pd nanoalloys represent an important class of catalysts for the oxidation of CO[9], decomposition of ethanol[10], reaction of the water-gas shift[11], and reduction of NO to N_2[12]. It has been shown that alloying Pd clusters with Cu greatly enhances their selectivity in the partial hydrogenation of dienes[13], and also extends the temperature range in which a high turnover rate for CO oxidation can be maintained. Due to the technological importance of Cu-Pd nanoalloys, a wide variety of experimental and theoretical investigations have been performed to elucidate their physical and chemical properties[14–17]. The knowledge about structure, composition, and segregation/mixing of nanoalloys is a very important guide for the understanding of their properties and mechanisms. Bulk Cu-Pd alloys, annealed or heat-treated below 500°C, can exist in three ordered phases: CuPd (bcc, B2), Cu_3Pd (fcc, L12), and Cu_4Pd (tetragonal)[18]; however, complex ordered and disordered behaviors are observed at

ISSN 2616-5880 Vol. 5, Issue 2: 29-36, DOI: 10.25236/AJMC.2024.050206

most catalytically relevant compositions[19,20]. Some conflicting results on the morphology and segregation of Cu-Pd alloys have been reported[21,22]. While earlier experimental investigations showed that Pd segregates to the surface of Cu-Pd alloy films[23], later Auger electron spectroscopy, low-energy ion spectroscopy, and theoretical calculations indicated that the top layer of the (100) surface of alloys is rich in Cu, whereas the composition of the (111) surface is close to that of the bulk alloy[24,25]. The analysis of Cu-Pd clusters by IR spectroscopy[26], X-ray scattering[21], and transmission electron microscopy[21], found substitution ally disordered Cu-Pd nanoalloys, different from perfectly ordered bcc-B2 structures shown in other transmission electron microscopy and high-resolution electron microscopy studies[27]. In addition, the degree of segregation in Cu-Pd clusters was also observed to be surface-dependent[21] .

They have also been explored for applications in fuel cells[28], sensors[29], and electronic devices, where its unique properties can be exploited. The synthesis of Cu-Pd CSNPs typically involves colloidal methods, such as seed-mediated growth[30], galvanic replacement[31], or electrochemical deposition[32], which allow for precise control over the core size, the shell thickness, and overall nanoparticle morphology.

In this work, we systematically investigated the 13- and 55- atom Cu and Pd NPs, and Cu-Pd CSNPs by DFT calculations. The purposes were to elucidate their geometries, electronic structures, and charge transfer, in particular, to determine the stability of the core–shell structures and to elucidate the crucial factor(s) for stabilizing the core-shell structures.

2. Computational methodology

All spin-polarized DFT calculations were performed with the Vienna Ab Initio simulation package (VASP)[33]. The exchange-correlation function was processed using the generalized gradient approximation (GGA) formulated by the Perdew-Burke-Ernzerhof (PBE)[34]. The interaction between the atomic core and electrons was explained by the Projector Augmented Wave method[35,36]. The energy cutoff for the plane-wave basis set was set to 400 eV. A 1×1×1 k-point mesh was used for all of the reciprocal space integration in all calculations due to its discrete nature. To prevent interaction between a cluster and its image, periodic boundary conditions were implemented with a minimum vacuum of 10 Å. The simulation boxes were 15×15×15 Å for smaller systems and 20×20×20 Å for larger systems. The atomic Bader charge analysis was used to calculate the global transferred charge[37,38].

3. Results and discussion

3.1. Structures of Cu, Pd NPs and Cu–Pd CSNPs

3.1.1. 13-Atom Cu, Pd NPs and Cu–Pd CSNPs

Based on experimental and theoretical studies of thermodynamic stability[39–43], the highly symmetric icosahedral structure was adopted for the 13- and 55-atom Cu, Pd NPs and Cu-Pd CSNPs, as this geometric structure is a local minimum in this size range. In addition, this structure is often tested in various theoretical studies. Figures 1 and 2 show the optimized structures for 13- and 55-atom Cu, Pd NPs and Cu/Pd CSNPs, and detailed results of the geometric structure parameters are given in Table 1. To simplify the notation, Am@Bn is used to represent a two-shell configuration with m A atoms in the core and n B atoms on the surface shell, and B@A_{m-1}@Bn is used to denote a three-shell configuration with one B atom in the center, m-1 A atoms in the inner shell, and n B atoms on the outermost surface shell.

Figure 1 shows the optimized structures of 13-Cu, Pd NPs and Cu-Pd CSNPs. For the monometallic Cu_{13} and Pd_{13}, the geometry is icosahedral due to the lowest energy in comparison to other structures. Both Cu_{13} and Pd_{13} have one atom in the core and 12 identical surface-shell atoms with a coordination number 6, as shown in Figures 1(a) and 1(b). The inter-atomic distances between the center and its neighboring 12 identical surface-shell atoms are 2.41 and 2.65 Å for Cu_{13} and Pd_{13} respectively, and the surface Cu-Cu and Pd-Pd bond lengths are 2.54 and 2.79 Å respectively.

Based on the monometallic Cu_{13} and Pd_{13} icosahedral structures, bimetallic 13-atom CSNPs, Pd@Cu_{12} and Cu@Pd_{12}, are constructed as shown in Figure 1(c) and 1(d). Compared to the monometallic Cu_{13} and Pd_{13} NPs, the geometry of the Pd@Cu_{12} and Cu@Pd_{12} configurations shows a

ISSN 2616-5880 Vol. 5, Issue 2: 29-36, DOI: 10.25236/AJMC.2024.050206

slight change. For $Pd@Cu_{12}$, the interatomic distance between the central Pd and 12 identical surface-shell Cu atoms is 2.48 Å, which is 0.07 Å longer than that of Cu_{13}, while the surface Cu-Cu bond length is 2.61 Å, which is longer than that of Cu_{13} by 0.07 Å. Similarly, for $Cu@Pd_{12}$, the distance between the center Cu and 12 identical surface-shell Pd atoms is 2.60 Å, and the surface Pd-Pd bond length is 2.73 Å, which is shorter than that of Pd_{13} by 0.05 Å and 0.06 Å, respectively.

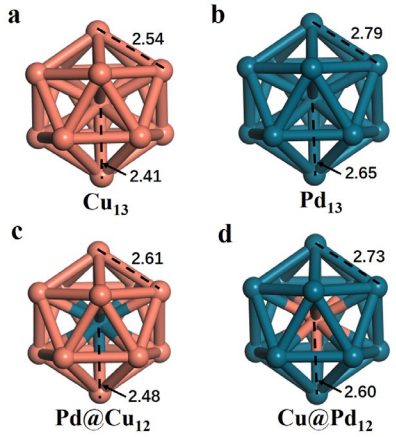

Figure 1: Schematic optimized structures of 13-atom monometallic Cu/Pd NPs and bimetallic Cu/Pd CSNPs. Bond lengths are given in angstroms.

3.1.2. 55-Atom Cu, Pd NPs and Cu–Pd CSNPs

As shown in Figure 2a and 2b, icosahedral Cu_{55} and Pd_{55} have one atom in the center, 12 atoms in the inner shell and 42 atoms in the surface shell, which can be generated by adding 42 Cu and Pd atoms on the surface of Cu_{13} and Pd_{13}, respectively. Thus, similar to the icosahedral Cu_{13} cluster, the interatomic distance in Cu_{55} between the center atom and the surrounding 12 neighbors in the inner shell is 2.44 Å. The surface shell atoms can be classified into two types of non-equivalent atoms related to the center atom of Cu_{55}. The first group has 12 identical atoms at the vertex positions of the Cu_{55} (referred to as "vertex atoms" in Figure 2a). They are 4.81 Å distant from the center atom and have a coordination number of 6. The other group has 30 identical atoms at edge positions with coordination number 8 (referred to as "edge atoms" in Figure 2a) and they are 4.21 Å away from the center atom. The surface Cu-Cu bond lengths are approximately 2.60 Å between two edge atoms and 2.53 Å for adjacent vertex and edge atoms. In the case of Pd_{55}, the interatomic distance between the center atom and the surrounding 12 adjacent atoms in the inner shell is 2.64 Å. The distances from 12 vertex and 30 edge atoms to the center atom are 5.30 and 4.58 Å respectively. The surface Pd-Pd bond lengths are approximately 2.79 Å between two edge atoms and 2.88 Å for adjacent vertex and edge atoms.

For 55-atom two-shell CSNPs, $Pd_{13}@Cu_{42}$ and $Cu_{13}@Pd_{42}$ configurations can be constructed from the monometallic Cu_{55} and Pd_{55} by swapping the 13 inner core atoms, as shown in Figure 2c and d. Compared to the corresponding Cu_{55} and Pd_{55}, the surface shell and inner shell of $Pd_{13}@Cu_{42}$ and $Cu_{13}@Pd_{42}$ show a significant change in geometrical structures. For $Pd_{13}@Cu_{42}$, the interatomic distance from the core atom to the 12-middle shell Pd atoms is 2.66 Å, which is 0.22 Å longer than that of Cu_{55}. The interatomic distances from the center Pd atom to the surface shell vertex and edge Cu atoms are 5.08 Å and 4.39 Å, respectively. The surface Cu-Cu bond lengths between two adjacent edge atoms and adjacent vertex and edge atoms are 2.72 and 2.67 Å, which are 0.12 and 0.14 Å longer than those of Cu_{55}, respectively. For $Cu_{13}@Pd_{42}$, the interatomic distances from the center Cu atom to 12 middle shell Cu atoms are 2.47 Å, which is 0.17 Å shorter than that of Pd_{55}. The interatomic distances from the center Cu atom to the surface shell vertex and edge Pd atoms are 5.13 Å and 4.42 Å, respectively. The surface Pd-Pd bond lengths between two adjacent edge atoms and adjacent vertex and edge atoms are 2.73 and 2.70 Å, which are 0.10 and 0.09 Å shorter than those of Pd_{55}, respectively.

ISSN 2616-5880 Vol. 5, Issue 2: 29-36, DOI: 10.25236/AJMC.2024.050206

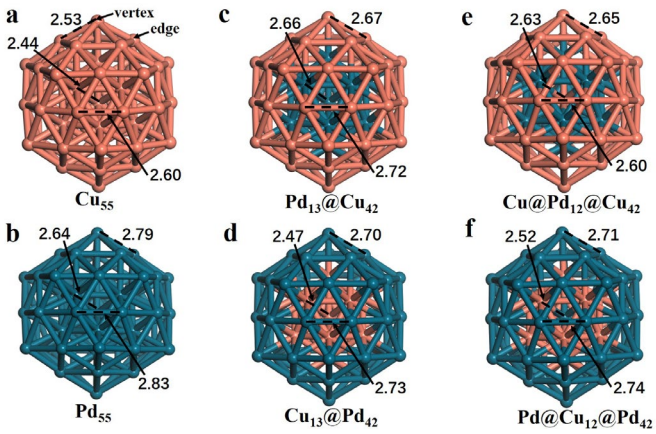

Figure 2: Optimized structures of 55-atom Cu, Pd NPs and two- and three-shell Cu-Pd CSNPs. Orange and blue spheres represent Cu and Pd atoms respectively. Bond lengths are given in angstroms.

The three-shell $Cu@Pd_{12}@Cu_{42}$ and $Pd@Cu_{12}@Pd_{42}$ CSNPs, similar to the $Pd_{13}@Cu_{42}$ and $Cu_{13}@Pd_{42}$ two-shell nanoparticles, can be further modeled by exchanging with each other the core atoms of the two-shell $Pd_{13}@Cu_{42}$ and $Cu_{13}@Pd_{42}$ CSNPs, as shown in Figure 3e and 3f. The two three-shell nanoparticles are only slightly different in geometry from the corresponding two-shell nanoparticles.

Table 1: Calculated results of total and excess of monometallic Cu, Pd NPs, and bimetallic Cu–Pd CSNPs

Nanoparticles	Etotal (eV)	Eexcess (eV)
Cu_{13}	-32.21176972	0.00
$Pd@Cu_{12}$	-33.28478633	-0.26
$Cu@PdCu_{11}$	-33.97036140	-0.95
Pd_{13}	-42.75378266	0.00
$Cu@Pd_{12}$	-45.27432789	-3.30
$Pd@CuPd_{11}$	-48.21911425	-6.28
Cu_{55}	-169.46363614	0.00
$Pd_{13}@Cu_{42}$	-180.18379000	0.77
$Pd_{12}Cu@Cu_{41}Pd^{e}$	-185.09356818	-4.14
$Pd_{12}Cu@Cu_{41}Pd^{v}$	-185.2280277	-4.28
$Cu_{13}@Pd_{13}Cu_{29}$	-193.06611773	-12.12
$Cu@Pd_{12}@Cu_{42}$	-180.28311821	0.67
Pd_{55}	-218.06050715	0.00
$Cu_{13}@Pd_{42}$	-221.60235066	-15.03
$Cu_{12}Pd@Pd_{41}Cu^{e}$	-228.55589511	-21.98
$Cu_{12}Pd@Pd_{41}Cu^{v}$	-228.26084027	-21.69
$Pd_{13}@Cu_{13}Pd_{29}$	-224.99744309	-18.43
$Pd@Cu_{12}@Pd_{42}$	-222.16878125	-15.60

3.2. Relative stability of the Cu–Pd CSNPs

In order to compare the relative stability of these NPs, the excess energy (E_{exc}) of $A_m@B_n$, $B@A_{m-1}@B_n$, or $A_{m-1}B@B_{n-1}A$ CSNPs is defined as follows[44,45]:

$$E_{exc} = E_{A_m@B_n/B@A(m-1)@B_n/A_{(m-1)}B@B_{(n-1)}A} - \frac{m}{n+m}E_{A_{(m+n)}} - \frac{n}{n+m}E_{B_{(n+m)}} \quad (1)$$

where $E_{Am@Bn/B@Am-1@Bn/Am-1B@Bn-1A}$, E_{Am+n}, and E_{Bn+m} are the total energies of bimetallic CSNPs and monometallic NPs A and B with the same size (m + n atoms) and geometry structures, respectively. In this study, the excess energy (Eexc) of the monometallic NPs is set to zero as a reference to benchmark that of the corresponding bimetallic CSNPs, a negative value of Eexc indicates in general an energetically favorable configuration.

ISSN 2616-5880 Vol. 5, Issue 2: 29-36, DOI: 10.25236/AJMC.2024.050206

The excess energy results in Figure 3 and Table I show that the relative stabilities of these Cu-Pd CSNPs follow the order Cu_{13}/Pd_{13}(0.00 eV) < $Pd@Cu_{12}$(-0.26 eV) < $Cu@Pd_{12}$(−3.30 eV) (see Figure 3a), and $Pd_{13}@Cu_{42}$(0.77 eV) < $Cu@Pd_{12}@Cu_{42}$(0.67 eV) < Cu_{55}/Pd_{55}(0.00 eV) < $Cu_{13}@Pd_{42}$(-15.03 eV) < $Pd@Cu_{12}@Pd_{42}$(-15.60 eV) (see Figure 3b). The results indicate that the Cu@Pd CSNPs with a Pd surface shell have lower excess energies, even lower than the corresponding monometallic NPs of Cu_{13}/Cu_{55} and Pd_{13}/Pd_{55}. Interestingly, Figure 3b shows that the three-shell $Pd@Cu_{13}@Pd_{42}$ has a lower excess energy than the two-shell $Cu_{13}@Pd_{42}$ by -0.57 eV, while the two-shell $Pd_{13}@Cu_{42}$ has a higher excess energy than the three-shell $Cu@Pd_{12}@Cu_{42}$ by 0.10 eV. These results indicate that the Cu@Pd CSNPs with a Pd surface shell are thermodynamically more favorable than the Cu@Pd CSNPs with a Cu surface shell. For the bimetallic Cu@Pd CSNPs, Pd atoms prefer to segregate to the surface, while Cu atoms tend to enrich in the inner shells.

In general, the surface sites in the bimetallic nanoparticles tend to be occupied by elements with lower surface energies. However, as the size of the bimetallic CSNPs decreases to 1 nm in diameter, it is not so easy to establish the prior existence of surface segregation in favor of a particular species due to various factors such as size-induced quantum size effects (i.e. electron confinement and surface effect). Thus, the segregation isomers of two-shell nanoparticles were further explored. For 13-atom CSNPs, there are two isomers, $Cu@PdCu_{11}$ and $Pd@CuPd_{11}$, by swapping an inner atom with a random surface atom. Figure 3a and Table I show that the $Pd@CuPd_{11}$ has a lower excess energy than the $Cu@Pd_{12}$, while $Pd@Cu_{12}$ is less stable than $Cu@PdCu_{11}$.

For the 55-atom $Pd_{13}@Cu_{42}$ with a complete Cu surface shell, three possible segregation isomers have been considered, (1) $Pd_{12}Cu@Cu_{41}Pd^{v}$ by swapping one inner Pd atom with a surface Cu vertex atom, (2) $Pd_{12}Cu@Cu_{41}Pd^{e}$ by swapping one inner Pd atom with a surface Cu edge atom, and (3) $Cu_{13}@Pd_{13}Cu_{29}$ by swapping 13 inner Pd atoms with a random surface Cu edge atom and 12 surface Cu vertex atoms. Similarly, three segregation isomers, $Cu_{12}Pd@Pd_{41}Cu^{v}$, $Cu_{12}Pd@Pd_{41}Cu^{e}$, and $Pd_{13}@Cu_{13}Pd_{29}$, have also been considered for the $Cu_{13}@Pd_{42}$ with a complete Pd surface-shell.

Table 1 shows that $Cu_{13}@Pd_{42}$ has the highest total energy of −221.60 eV, while the $Cu_{12}Pd@Pd_{41}Cue$ has the lowest total energy of −228.56 eV. The $Cu_{13}@Pd_{13}Cu_{29}$ has the lowest total energy of -193.07 eV, followed by $Pd_{12}Cu@Cu_{41}Pd^{e}$ (-185.09 eV) and $Pd_{12}Cu@Cu_{41}Pd^{v}$ (-185.23 eV). This is due to the replacement of surface Cu atoms by internal Pd atoms. These results further indicate that, for the bimetallic Cu-Pd CSNPs, the Pd atoms prefer to segregate to the surface shell, while the Cu atoms prefer to assemble in the core region.

Table 2: Bader charges of the 13-, 33- and 55-atom Cu, Pd NPs and Cu-Pd CSNPs.

Nanoparticle net charge	Inner core	Middle shell	Surface shell
Cu_{13}	+0.17	-	-0.17
$Pd@Cu_{12}$	-0.16	-	+0.16
$Cu@Pd_{12}$	+0.35	-	-0.35
Pd_{13}	+0.14	-	-0.14
Cu_{55}	-0.06	+0.89	-0.83
$Pd_{13}@Cu_{42}$	+0.21	-1.69	+1.48
$Cu@Pd_{12}@Cu_{42}$	+0.26	-2.47	+2.21
$Cu_{13}@Pd_{42}$	-0.04	+2.87	-2.83
$Pd@Cu_{12}@Pd_{42}$	-0.50	+3.27	-2.77
Pd_{55}	-0.04	+0.95	-0.91

3.3. Charge transfer in the Cu NP and Cu–Pd CSNPs

For bimetallic CSNPs, the heteronuclear metal atoms with different electronegativities may further enhance the charge transfer between inner and surface atoms. Additionally, the charge density on the surface-shell of bimetallic CSNPs may change noticeably when the inner-core and surface-shell atoms are exchanged. Therefore, charge transfer is further investigated using Bader charge analysis and the results are listed in Table 2. In this study, negative Bader charge corresponds to net charge accumulation, and positive Bader charge indicates net charge depletion on the core–shell atoms.

ISSN 2616-5880 Vol. 5, Issue 2: 29-36, DOI: 10.25236/AJMC.2024.050206

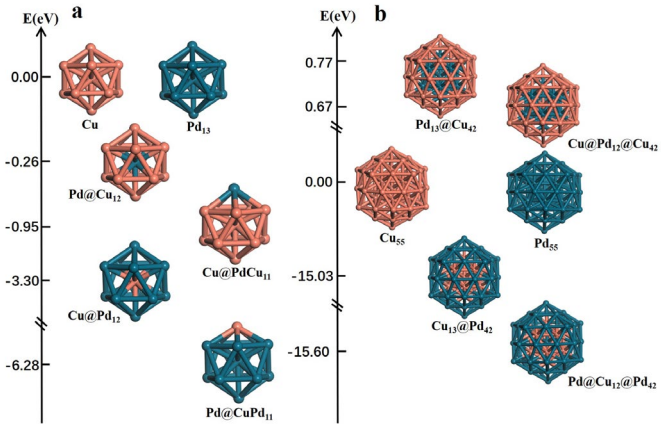

Figure 3: The excess energies of (a) 13- and (b) 55-atom Cu, Pd, NPs, and Cu-Pd CSNPs. Orange and blue spheres represent Cu and Pd atoms respectively.

In general, for monometallic NPs, there is a tendency for electron transfer from core atoms to surface atoms due to the surface effect. For 13-atom monometallic NPs, the net charge transfer from one core atom to 12 surface-shell atoms is 0.17 electron (e) for Cu_{13} and 0.14e for Pd_{13}. For monometallic NPs with 55 atoms, the charge is transferred from 12 middle shell atoms to the core atom and 42 outer shell atoms. The charge distributions of Cu_{55} are -0.06, +0.89 and -0.83e for the core, middle shell and surface shell atoms respectively. Similarly, the charge distributions of the Pd_{55} are−0.04, +0.95, and −0.91e for the core, middle-shell, and surface-shell atoms, respectively.

The large electronegativity difference between Cu (1.90) and Pd (2.20) would further enhance Cu to Pd electron transfer in the CSNP heterojunction[46]. The charge transfer of these Cu-Pd CSNPs is shown in Table 2. It can be seen that the charge is always transferred from the Cu atoms to the Pd atoms. Furthermore, due to the synergistic effects of surface and electronegativity, when Pd is on the surface and Cu is on the inner shell, charge transfer from Cu to Pd would be enhanced. For the 13-atom $Cu@Pd_{12}$, the net charge of 0.35e is transferred from the one Cu core atom to 12 surface-shell Pd atoms, resulting in a surface-shell that is 0.21e more negative than that of Pd_{13}. For the two-shell $Cu_{13}@Pd_{42}$, the charge transfer would further increase compared to that of Pd_{55} by 1.92e. The net charge of 2.83e is transferred from 13 Cu inner atoms to 42 Pd surface atoms. For the three-shell $Pd@Cu_{12}@Pd_{42}$, modeled from $Cu_{13}@Pd_{42}$ by swapping the one Cu core-atom with a Pd atom, the net charges of 0.50 and 2.77e are transferred from 12 Cu middle-shell atoms to the one core and 42 Pd surface atoms, respectively. For the $Pd_{13}@Cu_{42}$, one Pd core atom and 42 Cu surface atoms transfer the net charges of 0.21 and 1.48e to the 12 middle-shell Pd atoms, respectively, leading to a more positive surface-shell with + 1.48 e. Furthermore, for the $Cu@Pd_{12}@Cu_{42}$, one Cu core atom and 42 Cu surface atoms transfer the net charges of 0.26 and 2.21e to the 12 middle-shell Pd atoms, respectively.

4. Conclusions

In this work, the geometrical structure, thermodynamic stability and electronics of the 13- and 55-atom Cu, Pd, and Cu–Pd CSNPs were systematically studied using DFT calculations. Compared to the monometallic NPs, the change in the geometry was slight for the 13-atom CSNPs. Interestingly, for the 55-atom CSNPs, the surface shell and inner shell of $Pd_{13}@Cu_{42}$ and $Cu_{13}@Pd_{42}$ showed a significant change in geometrical structures. By contrast, the change of in the geometry was negligible for the $Cu@Pd_{12}@Cu_{42}$ and $Pd@Cu_{12}@Pd_{42}$ CSNPs. The total and excess energies evidenced that the relative thermodynamic stabilities of these NPs followed the order Cu_{13}/Pd_{13} < $Pd@Cu_{12}$ < $Cu@Pd_{12}$ for 13-atom systems and $Pd_{13}@Cu_{42}$ < $Cu@Pd_{12}@Cu_{42}$ < Cu_{55}/Pd_{55} < $Cu_{13}@Pd_{42}$ < $Pd@Cu_{12}@Pd_{42}$. These results implied that in the bimetallic Cu-Pd CSNPs, Pd atoms preferred to segregate to the surface shell, while Cu atoms preferred to assemble in the core region. The Cu@Pd CSNPs with a Pd surface shell were thermodynamically more favorable than both the monometallic Cu/Pd NPs and the Pd@Cu CSNPs with a Cu surface shell. Bader charge analysis showed that the charge transfer increased from the Cu-core to the Pd-shell for the Cu@Pd CSNPs, while it decreased from the Pd-core to the Cu-shell for the Pd@Cu CSNPs. Opposite charge transfer in these CSNPs led to the Pd surface-shell that displaying a negative charge, while the Cu surface-shell exhibited a positive charge.

ISSN 2616-5880 Vol. 5, Issue 2: 29-36, DOI: 10.25236/AJMC.2024.050206

Acknowledgements

This work was supported by the Fundamental Research Funds for the Universities of Henan Province (NSFRF140129) and the Doctor Foundation of Henan Polytechnic University (B2008-71).

References

[1] Wei S, Wang Q, Zhu J, et al. Multifunctional composite core–shell nanoparticles[J]. Nanoscale, 2011, 3(11): 4474-4502.
[2] Sun Q, Zhang X Q, Wang Y, et al. Recent progress on core-shell nanocatalysts[J]. Chinese Journal of Catalysis, 2015, 36(5): 683-691.
[3] Gawande M B, Goswami A, Asefa T, et al. Core–shell nanoparticles: synthesis and applications in catalysis and electrocatalysis[J]. Chemical Society Reviews, 2015, 44(21): 7540-7590.
[4] Henning A M, Watt J, Miedziak P J, et al. Gold–Palladium Core–Shell Nanocrystals with Size and Shape Control Optimized for Catalytic Performance[J]. Angewandte Chemie International Edition, 2013, 52(5): 1477-1480.
[5] Vysakh A B, Babu C L, Vinod C P. Demonstration of Synergistic Catalysis in Au@Ni Bimetallic Core–Shell Nanostructures[J]. The Journal of Physical Chemistry C, 2015, 119(15): 8138-8146.
[6] Guisbiers G, Khanal S, Ruiz-Zepeda F, et al. Cu–Ni nano-alloy: mixed, core–shell or Janus nano-particle [J]. Nanoscale, 2014, 6(24): 14630-14635.
[7] Feng X, Shi D, Jia J, et al. Structural, mixing, electronic and magnetic properties of small Cu-Pd nanoalloy clusters[J]. Materials Today Communications, 2022, 31: 103222.
[8] Wu X, Zhang Y. Structural differences of Cu-Pd clusters with three potential parameters[J]. Chemical Physics Letters, 2024, 842: 141200.
[9] Choi K I, Vannice M A. CO oxidation over Pd and Cu catalysts V. Al_2O_3-supported bimetallic Pd-Cu particles[J]. Journal of Catalysis, 1991, 131(1): 36-50.
[10] Mierczynski P, Vasilev K, Mierczynska A, et al. Highly selective Pd–Cu/$ZnAl_2O_4$ catalyst for hydrogen production[J]. Applied Catalysis A: General, 2014, 479: 26-34.
[11] Greeley J, Nørskov J K, Kibler L A, et al. Hydrogen Evolution Over Bimetallic Systems: Understanding the Trends[J]. ChemPhysChem, 2006, 7(5): 1032-1035.
[12] Feilong Xing, Jaewan Jeon, Takashi Toyao, Ken-ichi Shimizu, and Shinya Furukawa. A Cu–Pd single-atom alloy catalyst for highly efficient NO reduction [J]. Chemical Science, 2019, 10(36): 8292-8298.
[13] Phillips J, Auroux A, Bergeret G, et al. Phase behavior of palladium-silver particles supported on silica [J]. The Journal of Physical Chemistry, 1993, 97(14): 3565-3570.
[14] Alvarez-Garcia A, Flórez E, Moreno A, et al. CO2 activation on small Cu-Ni and Cu-Pd bimetallic clusters [J]. Molecular Catalysis, 2020, 484: 110733.
[15] Gómez Herranz A, Germán E, Alonso J A, et al. Interaction of hydrogen with palladium–copper nanoalloys[J]. Theoretical Chemistry Accounts, 2021, 140(4): 35.
[16] Luna-Valenzuela A, Cabellos J L, Alonso J A, et al. Effects of van der Waals interactions on the structure and stability of Cu8-xPdx (x = 0, 4, 8) cluster isomers[J]. Materials Today Communications, 2021, 26: 102024.
[17] Chen D, Wang Y, Liu D, et al. Surface composition dominates the electrocatalytic reduction of CO 2 on ultrafine CuPd nanoalloys[J]. Carbon Energy, 2020, 2(3): 443-451.
[18] Geisler A H, Newkirk J B. Ordering Reaction of the Cu4Pd Alloy[J]. JOM, 1954, 6(9): 1076-1082.
[19] Paniago R, de Siervo A, Soares E A, et al. Pd growth on Cu (111): stress relaxation through surface alloying [J]. Surface Science, 2004, 560(1): 27-34.
[20] Canzian A, Mosca H O, Bozzolo G. Surface alloying of Pd on Cu (111) [J]. Surface Science, 2004, 551(1): 9-22.
[21] Zhu L, Liang K S, Zhang B, et al. Bimetallic Pd–Cu Catalysts: X-Ray Diffraction and Theoretical Modeling Studies[J]. Journal of Catalysis, 1997, 167(2): 412-416.
[22] Montejano-Carrizales J M, I.Iguez M P, Alonso J A. Embedded-atom method applied to bimetallic clusters: The Cu-Ni and Cu-Pd systems[J]. Physical Review B Condensed Matter, 1994, 49(23): 16649.
[23] van Langeveld A D, Hendrickx H A C M, Nieuwenhuys B E. The surface composition of Pd-Cu alloys: A comparative investigation of photoelectric work function measurements, Auger electron spectroscopy and calculations based on a broken bond approximation[J]. Thin Solid Films, 1983, 109(2): 179-192.
[24] Miller J B, Matranga C, Gellman A J. Surface segregation in a polycrystalline $Pd_{70}Cu_{30}$ alloy hydrogen purification membrane[J]. Surface Science, 2008, 602(1): 375-382.

ISSN 2616-5880 Vol. 5, Issue 2: 29-36, DOI: 10.25236/AJMC.2024.050206

[25] Jl. R, Miegge P, Jc. B. Theory of segregation using the equivalent-medium approximation and bond-strength modifications at surfaces: Application to fcc Pd-X alloys. [J]. Physical Review.B.Condensed Matter, 1996(8): 53.

[26] Fernández-García M, Anderson J A, Haller G L. Alloy Formation and Stability in Pd−Cu Bimetallic Catalysts[J]. The Journal of Physical Chemistry, 1996, 100(40): 16247-16254.

[27] Gai P L, Smith B C. Dynamic electron microscopy of copper-palladium intermetallic compound catalysts [J]. Ultramicroscopy, 1990, 34(1): 17-26.

[28] Xuan J, Hong W, Chuannan G. Preparation of Core-Shell Cu@Pt-Pd Electrode for Fuel Cells by High Temperature Reduction of Ethylene Glycol[J]. Yunnan Chemical Technology, 2019.

[29] Yang C L, Zhang X H, Lan G, et al. Pd-based nanoporous metals for enzyme-free electrochemical glucose sensors [J]. China ChemExpress: English version, 2014(4): 496-500.

[30] Calabro R L, Burpo F J, Bartolucci S F, et al. Seed-Mediated Growth of Oxidation-Resistant Copper Nanoparticles[J]. The Journal of Physical Chemistry C, 2023, 127(31): 15307-15315.

[31] Tang Z, Han G H, Jung E, et al. Synthesis of Cu-Pd nanoplates and their catalytic performance for H_2O_2 generation reaction[J]. Molecular Catalysis, 2018, 452: 117-122.

[32] Allemand M, Martin Manuel H, Reyter D, et al. Synthesis of Cu–Pd alloy thin films by co-electrodeposition[J]. Electrochimica Acta, 2011, 56(21): 7397-7403.

[33] Kresse G, Furthmüller J. Efficiency of ab-initio total energy calculations for metals and semiconductors using a plane-wave basis set[J]. Computational Materials Science, 1996, 6(1): 15-50.

[34] Kresse G, Joubert D. From ultrasoft pseudopotentials to the projector augmented-wave method[J]. Physical Review B, 1999, 59(3): 1758-1775.

[35] Blöchl P E. Projector augmented-wave method[J]. Physical Review B, 1994, 50(24): 17953-17979.

[36] Perdew J P, Burke K, Ernzerhof M. Generalized Gradient Approximation Made Simple[J]. Physical Review Letters, 1996, 77(18): 3865-3868.

[37] Sanville E, Kenny S D, Smith R, et al. Improved grid-based algorithm for Bader charge allocation [J]. Journal of Computational Chemistry, 2007, 28(5): 899-908.

[38] Henkelman G, Arnaldsson A, Jónsson H. A fast and robust algorithm for Bader decomposition of charge density [J]. Computational Materials Science, 2006, 36(3): 354-360.

[39] Yang Z, Wang Q, Shan X, et al. DFT study of Fe-Ni core-shell nanoparticles: Stability, catalytic activity, and interaction with carbon atom for single-walled carbon nanotube growth[J]. The Journal of Chemical Physics, 2015, 142(7): 074306.

[40] Xiang Y, Sun D Y, Gong X G. Generalized Simulated Annealing Studies on Structures and Properties of Nin (n = 2−55) Clusters[J]. The Journal of Physical Chemistry A, 2000, 104(12): 2746-2751.

[41] Singh R, Kroll P. Structural, electronic, and magnetic properties of 13-, 55-, and 147-atom clusters of Fe, Co, and Ni: A spin-polarized density functional study[J]. Physical Review B, 2008, 78(24): 245404.

[42] Knickelbein M B. Electric dipole polarizabilities of Ni12–58[J]. The Journal of Chemical Physics, 2001, 115(13): 5957-5964.

[43] Böyükata M, Belchior J C. Structural and energetic analysis of copper clusters: MD study of Cu n (n = 2-45) [J]. Journal of the Brazilian Chemical Society, 2008, 19(5): 884-893.

[44] Sahoo S, Rollmann G, Entel P. Segregation and ordering in binary transition metal clusters[J]. Phase Transitions, 2006, 79(9-10): 693-700.

[45] Ferrando R, Jellinek J, Johnston R L. Nanoalloys: From Theory to Applications of Alloy Clusters and Nanoparticles [J]. Chemical Reviews, 2008, 108(3): 845-910.

[46] Allred A L. Electronegativity values from thermochemical data[J]. Journal of Inorganic and Nuclear Chemistry, 1961, 17(3): 215-221.